ACTA ONCOLOGICA
2023, VOL. 62, NO. 2, 141–149
https://doi.org/10.1080/0284186X.2023.2176254

Taylor & Francis
Taylor & Francis Group

ORIGINAL ARTICLE

Unchanged perfusion in normal-appearing white and grey matter of glioma patients nine months after proton beam irradiation

Katharina Witzmann[a,b], Felix Raschke[a,b], Steffen Löck[b,c,d,e], Tim Wesemann[f], Mechthild Krause[a,b,c,d,e], Jennifer Linn[e,f] and Esther G. C. Troost[a,b,c,d,e]

[a]Helmholtz-Zentrum Dresden-Rossendorf, Institute of Radiooncology – OncoRay, Dresden, Germany; [b]OncoRay - National Center for Radiation Research in Oncology, Faculty of Medicine and University Hospital Carl Gustav Carus, Technische Universität Dresden, Helmholtz-Zentrum Dresden-Rossendorf, Dresden, Germany; [c]Department of Radiotherapy and Radiation Oncology, Faculty of Medicine and University Hospital Carl Gustav Carus, Technische Universität Dresden, Dresden, Germany; [d]German Cancer Consortium (DKTK), Partner Site Dresden, and German Cancer Research Center (DKFZ), Heidelberg, Germany; [e]National Center for Tumor Diseases (NCT), Partner Site Dresden, Germany: German Cancer Research Center (DKFZ), Heidelberg, Germany; Faculty of Medicine and University Hospital Carl Gustav Carus, Technische Universität Dresden, Dresden, Germany, and; Helmholtz Association / Helmholtz-Zentrum Dresden-Rossendorf (HZDR), Dresden, Germany; [f]Institute of Neuroradiology, University Hospital Carl Gustav Carus and Medical Faculty of Technische Universität, Dresden, Germany

ABSTRACT

Purpose: Radio(chemo)therapy is used as a standard treatment for glioma patients. The surrounding normal tissue is inevitably affected by the irradiation. The aim of this longitudinal study was to investigate perfusion alterations in the normal-appearing tissue after proton irradiation and assess the dose sensitivity of the normal tissue perfusion.

Methods: In 14 glioma patients, a sub-cohort of a prospective clinical trial (NCT02824731), perfusion changes in normal-appearing white matter (WM), grey matter (GM) and subcortical GM structures, i.e. caudate nucleus, hippocampus, amygdala, putamen, pallidum and thalamus, were evaluated before treatment and at three-monthly intervals after proton beam irradiation. The relative cerebral blood volume (rCBV) was assessed with dynamic susceptibility contrast MRI and analysed as the percentage ratio between follow-up and baseline image (ΔrCBV). Radiation-induced alterations were evaluated using Wilcoxon signed rank test. Dose and time correlations were investigated with univariate and multivariate linear regression models.

Results: No significant ΔrCBV changes were found in any normal-appearing WM and GM region after proton beam irradiation. A positive correlation with radiation dose was observed in the multivariate regression model applied to the combined ΔrCBV values of low (1–20 Gy), intermediate (21–40 Gy) and high (41–60 Gy) dose regions of GM ($p < 0.001$), while no time dependency was detected in any normal-appearing area.

Conclusion: The perfusion in normal-appearing brain tissue remained unaltered after proton beam therapy. In further studies, a direct comparison with changes after photon therapy is recommended to confirm the different effect of proton therapy on the normal-appearing tissue.

Abbreviations: AIF: arterial input function; ANTs: Advanced Normalisation Tools; ASL: arterial spin labeling; AUC: area under curve; CBF: cerebral blood flow; CBV: cerebral blood volume; CET1w: contrast enhanced T1w; CT: computed tomography; CTV: clinical target volume; DCE: dynamic contrast enhanced; DSC: dynamic susceptibility contrast; FLAIR: fluid attenuated inversion recovery; FSL: FMRIB Software Library; GM: grey matter; GTV: gross tumour volume; MRI: magnetic resonance imaging; NA: normal-appearing; PRESTO: Principles of Echo-Shifting with a Train of Observation; RBE: relative biological effectiveness; RD: radiation dose; ROI: region of interest; RT: radiotherapy; T1w: T1-weighted; T2w: T2-weighted; TBV: tumour bed volume; WM: white matter

ARTICLE HISTORY
Received 30 August 2022
Accepted 31 January 2023

KEYWORDS
Dynamic susceptibility contrast; relative cerebral blood volume; normal-appearing brain tissue; perfusion changes; proton beam irradiation; radio(chemo)therapy

Introduction

Radiotherapy is an essential component of the standard treatment of grade 2-4 gliomas, along with surgery and chemotherapy [1–4]. In radiotherapy of gliomas, the clinical target volume (CTV) is defined to ensure complete coverage of microscopic tumour extension. The CTV typically includes the resection cavity, areas of suspected proliferating tumour cells using a 1-2cm margin around contrast enhancements of T1-weighted (T1w) magnetic resonance imaging (MRI), acquired with a contrast agent, and areas of T2-weighted (T2w) hyperintensities to ensure the irradiation of potential tumour infiltration [5,6]. The enlargement of the irradiated region, positioning inaccuracies during treatment and the characteristics of different irradiation methods inevitably result in a certain radiation dose affecting the surrounding normal-appearing (NA) tissue. This can cause

CONTACT Esther G. C. Troost esther.troost@uniklinikum-dresden.de Department of Radiotherapy and Radiation Oncology, Faculty of Medicine and University Hospital Carl Gustav Carus of Technische Universität Dresden, Fetscherstrasse 74, 01307, Dresden, Germany

Supplemental data for this article can be accessed online at https://doi.org/10.1080/0284186X.2023.2176254.

anatomical changes such as demyelination and oedema in the NA tissue and may lead to functional damage to cognition or memory loss [7,8]. Noteworthy, a direct correlation between MR imaging changes in the NA tissue and cognitive impairment has not yet been demonstrated. The severity of the damage is categorised as acute, early delayed and late delayed, where acute and early delayed injuries are usually temporary and reversible, while late delayed effects are mostly irreversible and progressive [9]. The radiation exposure to the normal tissue can be significantly reduced with proton compared to photon irradiation, as protons deliver the dose mainly to the tumour and a close proximity [10]. Investigating whether the reduction of radiation exposure to NA tissue leads to a decrease in MR imaging changes and possibly fewer side-effects may impact on the decision regarding the radiation modality. Furthermore, since severe radiation-induced damage may occur with a time delay, the search for early biomarkers of late dysfunction is highly for patient selection. Previously, advanced MRI methods, e.g. diffusion imaging, perfusion imaging and MR spectroscopy, were used to specify the radiation-induced changes in the NA brain tissue [11–14] resulting in diffusion changes indicating demyelination and axonal loss [13] metabolic alterations suggesting changes on neuronal health [15], and reduced perfusion [16–18].

The perfusion alterations were mainly studied using dynamic susceptibility contrast (DSC) [16,17,19–21], but also with dynamical contrast enhancement (DCE) [22] and arterial spin labeling (ASL) [18,23]. Decreasing cerebral blood volume (CBV) and cerebral blood flow (CBF) in the NA white matter (WM) [16,17,19] and grey matter (GM) [16,18,23] appeared to be a common observation, although contradictory findings were detected [20]. Furthermore, dose-dependency of the perfusion changes was observed [16–18]. While in most of the previous studies the cohort consisted of photon-irradiated patients, the study of Petr et al. [23] evaluated perfusion and atrophy alterations in glioblastoma patients 3–6 months after treatment both after proton and photon therapy. Perfusion reduction in the whole GM appeared after photon irradiation, whereas no significant reduction in perfusion was observed in proton-irradiated patients.

The previous results indicate the relevance of investigating the radiation-induced behaviour of perfusion after proton therapy. Thus, the aim of this study was to analyse the effect of proton beam irradiation on the perfusion in NA brain tissue and to evaluate time- or dose-dependent variations. For this purpose, we determined the relative CBV using DSC-MRI in the normal-appearing WM, GM and subcortical GM structures of the entire brain and dose-bins. Since the effect of proton irradiation has been studied only to a limited extent, this work is believed to represent an important contribution to the understanding of the effect of proton therapy.

Material and methods

Patient cohort

MRI data from grade 2–4 glioma patients treated with adjuvant proton beam irradiation and chemotherapy following MRI-confirmed gross tumour resection were collected in a longitudinal study to monitor possible tissue changes indicative of radiation-induced alterations or tumour progression. The patient cohort represents a subgroup of a prospective clinical trial (NCT02824731) and was approved by the local Ethics Committee of the Technische Universität Dresden, Germany (EK22012016). Between 2016 and 2021, patients were included in this longitudinal study and received MR scans containing a baseline MRI measured approximately two weeks before radiotherapy (RT) and three-monthly MRI follow-up scans after RT. Each patient received at least one follow-up MRI. MRI scans with clear tumour progression were excluded from the analysis as were patients with a deteriorating performance status hampering MR acquisition to avoid a coincidence of these effects with the radiation-induced injury.

Data acquisition

The MR measurements were performed on a 3 T Philips Ingenuity PET/MR scanner (Philips, Eindhoven, The Netherlands) using an eight-channel head coil. T1w images were measured with a 3D gradient echo sequence with TR = 10 ms, TE = 3.7 ms, flip angle FA = 20° and voxel size $1 \times 1 \times 1$ mm^3 in sagittal orientation. 3D FLAIR images were acquired with TR = 4800 ms, TE = 293 ms, TI = 1650 ms, FOV = 250×250 mm, acquisition matrix 252×249, reconstruction matrix 512×512 and a reconstructed slice thickness of 0.5 mm in sagittal orientation. Perfusion was accessed via DSC imaging using a PRESTO sequence with TR = 15 ms, TE = 21 ms, voxel size $1.8 \times 1.8 \times 3.5$ mm^3 and 60 dynamics with a dynamic scan time of 1.7 s. Prior to DSC imaging, the intravenous contrast agent gadolinium (0.1 mol/kg, 4 ml/s, 7 s delay) was injected followed by a saline flush (20 ml, 4 ml/s) using an injector pump (MEDRAD Spectris Solaris EP). A pre-bolus gadolinium injection (0.1 mol/kg, 4 ml/s) was given in advance to avoid T1-leakage effects.

Radiation treatment planning

For radiation treatment planning, computed tomography (CT) scans were obtained in a supine patient position using an individual head support and a custom-made head mask. The CTs were registered to the post-surgery T1w, T2w and CET1w images to define the tumour bed volume (TBV) and possibly the gross tumour volume (GTV). The CTV was specified by expanding the TBV (and possibly the GTV) using a 1–2 cm isotropic margin and including the T2w image changes, taking into account the anatomical boundaries. The proton dose was prescribed to the CTV allowing for inherent uncertainties of the proton range. Either the pencil-beam scanning approach with uniform single-field dose optimisation or the double-scattering method with field shaping using lateral apertures and range compensators were used to deliver protons with a maximum beam energy of 230 MeV. The radiation dose was delivered in two to three radiation fields choosing a beam direction avoiding areas of high LET. A total dose of 54–60 Gy(RBE) in 27–30 fractions

was prescribed, taking into account a constant relative biological effectiveness (RBE) of 1.1.

Data processing

The CTV, planning CT, and radiation dose (RD) map was reconstructed from the planning workstation and rigidly registered to the baseline T1w scan using Advanced Normalisation Tools (ANTs) [24]. Baseline and follow-up images were aligned by a non-linear registration of the T1w maps being applied to the planning CT and RD map (for a detailed description of image registration, see the Supplementary Material of Raschke et al. [13]). The NA tissue was defined by excluding the CTV and abnormal areas indicative of tumour progression, identified as T2w hyperintensities on FLAIR (Figure 1(A)). The definition of normal tissue ensures that the changes are exclusively caused by the irradiation and not by tumour progression, such that non-visible radiation damages in advanced MRI can be detected. To exclude the same abnormal area in all follow-up scans, the abnormal areas of all time points were combined in every patient, and this individual abnormality mask was registered to each T1w scan. Areas showing strong B0-inhomogeneities were identified on a displacement map generated from opposite phase encoded diffusion-tensor imaging measurements and excluded from the analysis. The cerebellum and brainstem, defined by a cerebellar mask on the Montreal Neurological Institute (MNI) 152 6th generation atlas [25] from the FMRIB Software Library (FSL) [26], were excluded to avoid a difference in brain coverage due to varying spatial coverage of the MRI sequences. WM and GM tissue were segmented on the T1w images using SPM12 [27] and transformed to binary tissue masks using a 95%-probability threshold (Figure 1(B)). Subcortical GM structures were localised on the Harvard-Oxford subcortical structural atlas from FSL and

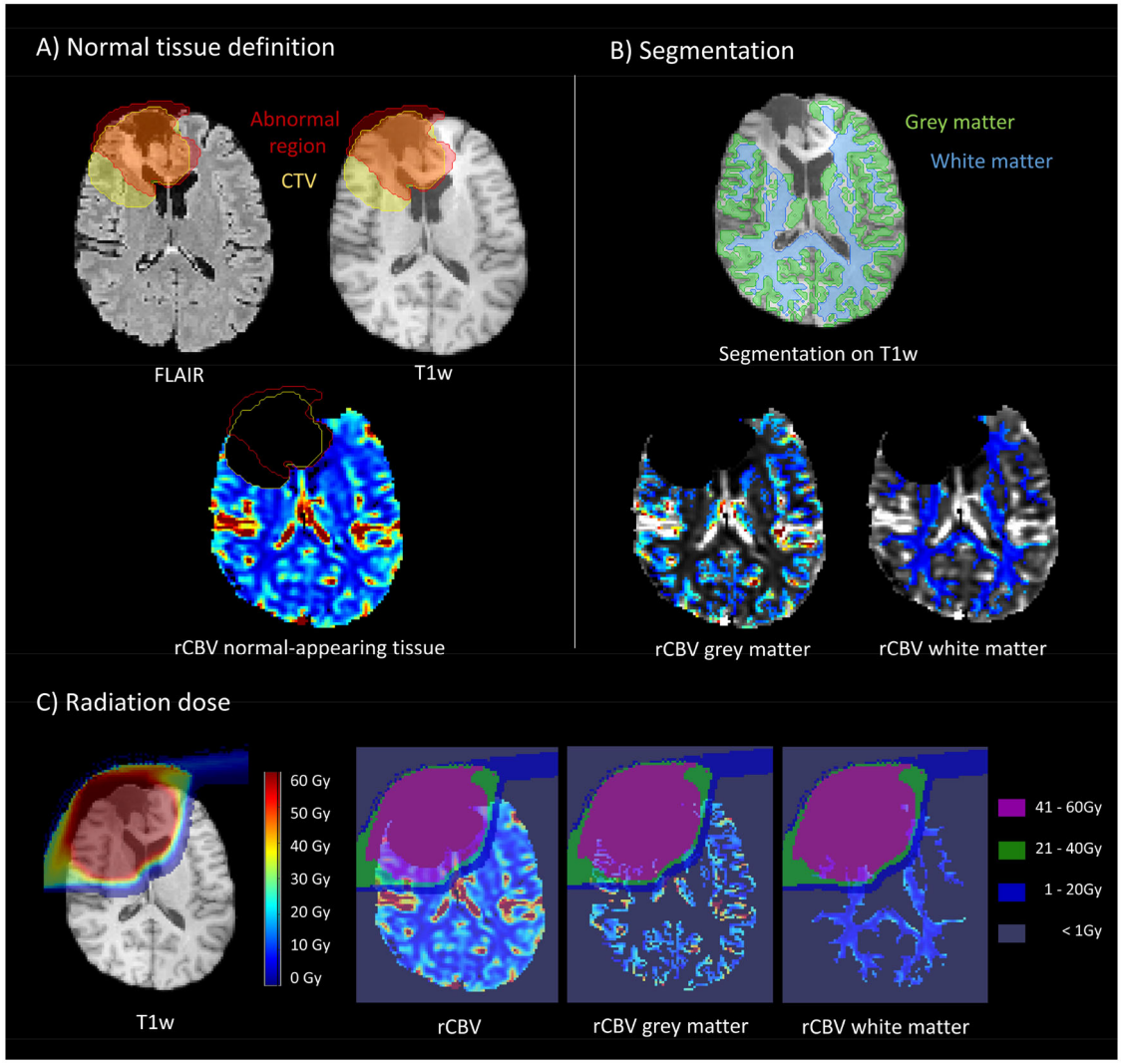

Figure 1. (A) Normal tissue definition by the exclusion of the clinical target volume (CTV) and the areas appearing abnormal on FLAIR imaging. (B) White and grey matter segmentation, defined on T1-weighted (T1w) magnetic resonance imaging (MRI) and registered to relative cerebral blood volume (rCBV) with Advanced Normalisation Tools (ANTs) [24]. (C) Dose distribution of proton irradiation – left: continuous radiation dose distribution, right: dose distribution divided into high dose [41–60 Gy(RBE), pink], intermediate dose [21–40 Gy(RBE), green], low dose [1–20 Gy(RBE), blue] and areas with negligible low radiation dose named "w/o-radiation" – area [<1 Gy(RBE), purple].

registered to the T1w image with ANTs [24–26]. Finally, the T1w image and the corresponding masks were rigidly registered to the calculated perfusion parameter map (CBV) using ANTs [24].

Data analysis

The signal information of the dynamic PRESTO measurements was converted to concentration-time curves on a voxel-wise basis [28,29]. The area under the curve (AUC) was determined by fitting a gamma variate function to the smoothed concentration-time curves [30]. The CBV was determined as the ratio of the AUC to the arterial input function (AIF) obtained with an in-house algorithm written in MATLAB based on the criteria of Mouridsen et al. and Yin et al. [31–33]. The relative (r)CBV was achieved by normalisation to a WM region of interest (ROI) receiving less than 1 Gy(RBE) [34]. The median rCBV values were evaluated in the entire NA tissue (0–60 Gy(RBE)), in areas receiving a negligible radiation dose ("w/o-radiation", 0–1 Gy(RBE)) and in areas exposed to radiation ("w/-radiation", 1–60 Gy(RBE)). The tissue exposed to radiation was further subdivided into three dose regions of low (1–20 Gy(RBE)), intermediate (21–40 Gy(RBE)) and high dose (41–60 Gy(RBE)) tissue of WM and GM (compare Figure 1(C)) to estimate the dose-dependency of radiation response, similar to previous studies [13,18,23]. Wider dose bins were chosen as the regions would otherwise contain relatively few voxels due to the steep dose gradient of proton irradiation and the low spatial resolution of DSC. Additionally, median rCBV was analysed in the subcortical GM structures caudate nucleus, hippocampus, amygdala, putamen, pallidum and thalamus, since different radiation-sensitivity of these structures has already been observed [35,36]. Subcortical GM structures containing voxels of abnormal tissue or overlapping with the CTV were excluded from the analysis. Moreover, this analysis was not performed in case data of less than two patients contributed to the cohort at the respective follow-up measurement. The percentage change (ΔrCBV) was calculated as the difference between follow-up and baseline rCBV normalised to the baseline perfusion:

$$\Delta rCBV = \frac{rCBV_{\text{follow-up}} - rCBV_{\text{baseline}}}{rCBV_{\text{baseline}}} \cdot 100$$

Statistical analyses

The first analysis focussed on the perfusion changes in several dose regions of the normal-appearing WM and GM. To identify patient-wise changes after RT, ΔrCBV was analysed with the one-sample Wilcoxon signed rank test in the entire region, "w/o-radiation"-area, "w/-radiation"-area and low, intermediate and high dose region of normal-appearing WM and GM. A p-value ≤ 0.05 was considered statistically significant. The paired Wilcoxon signed rank test was used to analyse ΔrCBV differences in between the low, intermediate and high dose perfusion. To counteract multiple comparison problems a Bonferroni correction factor of 3 was required, resulting in a corrected p-value ≤ 0.017 indicative of statistical significance. Univariate and multivariate linear regression models analysing the correlation of ΔrCBV with time since RT and mean dose per region, as well as the patient age, tumour grade, gender and treatment with chemotherapy were performed with the Statistical Package for Social Science (IBM SPSS Statistics) [37]. The linear regression was performed using generalised estimation equations accounting for the within-subject effects of multiple MRI follow-up measurements and different dose regions. The consideration of the dose areas as within-subject variables was only required when analysing the data set combining the results of low, intermediate and high dose regions. The work correlation matrix "autoregressive relationship AR(1)" was chosen in case of one factor acting as within-subject in the analysis, while "exchangeable" was selected in the case of two factors as within-subjects [37]. Univariate models analysed the correlation with the factors time, patient age, tumour grade, gender and treatment with chemotherapy in the WM and GM regions. The dose-correlation was not evaluated in regions subdivided according to the radiation dose. Multivariate linear mixed model was analysed on the combined low, intermediate and high dose dataset and considered the simultaneous effects of time, dose and additional parameters correlating significantly with ΔrCBV in the univariate model.

In a second analysis, the ΔrCBV changes in the subcortical GM structures were evaluated separately for the ipsi- and contralateral hemisphere relative to the primary tumour location. Time-dependent alterations on the ipsi- and contralateral side were determined using the one-sample Wilcoxon signed rank test. The paired Wilcoxon signed rank test was taken to compare the changes between the ipsi- and contralateral hemisphere. Univariate and multivariate linear regression models were applied to the dataset combining the information of the ipsi- and contralateral side of each subcortical GM structure.

Results

In total, 42 MRI scans of 14 patients with grade 2–4 primary brain tumours were available for the evaluation of perfusion changes, including the baseline MRI before RT as well as follow-up MRIs at three, six and nine months after RT (Table 1). The one-sided Wilcoxon signed rank test did not reveal significant ΔrCBV alterations between baseline and any follow-up measurement, neither in the entire normal-appearing WM/GM tissue nor in the dose-separated WM/GM areas (Figure 2). Analysing the time-dependency of ΔrCBV with the univariate linear regression model did not show significant correlations in any WM and GM region receiving a non-negligible radiation dose. Contrarily, in the region "w/o-irradiation" of WM, i.e. 0–1 Gy(RBE), perfusion correlated negatively with time (Suppl. Table S1). Comparing the perfusion of low, intermediate and high dose regions to one another revealed higher ΔrCBV values in the high compared to the intermediate dose GM region three months after RT ($p = 0.05$; Suppl. Table S2), considering

the uncorrected p-value. The univariate dose analysis of the combined dataset of low, intermediate and high dose ΔrCBV at each follow-up time-point showed a dose-correlation of 0.08%/Gy(RBE) three months after RT in GM ($p = 0.006$) but no correlation in WM (Suppl. Table S3). Since we found a significant dependency of ΔrCBV with the patients' gender in the univariate model of almost all regions (Suppl. Table S1), multivariate analysis was chosen to consider the correlated influence of time, radiation dose and gender and applied to the dataset combining low, intermediate and high dose region:

$$\Delta rCBV = a + b \times time + c \times dose + d \times gender + e \times time \times dose \times gender\ 'f' + f \times time \times dose \times gender\ 'm'$$

This analysis demonstrated that the dose-correlation in GM was significant ($p = 0.001$), indicating an increase in perfusion with radiation dose of 0.027%/Gy(RBE), whereas no significant findings were observed for WM (Table 2). A correlation with gender was seen in GM ($p = 0.02$) and WM ($p = 0.04$) as well as a significant but very small influence of time × dose × gender to ΔrCBV in GM (0.0004%/days × Gy(RBE); $p = 0.008$) and WM (-0.0004%/days × Gy(RBE); $p = 0.03$).

For the assessment of subcortical GM structures, the number of patients available was substantially decreased due to the complete exclusion of regions overlapping with abnormal tissue and the limited number of datasets at a given time point. The statistical analyses of the subcortical GM structures, apart from the excluded caudate nucleus, showed no significant changes, neither in ipsi- or contralateral ΔrCBV (Suppl. Table S4), nor for the comparison of ipsi- and contralateral perfusion (data not shown). No time-correlation was observed in the univariate regression model, whereas some structures showed significant correlations with age, gender and tumour grade (Table 3). Due to the small patient numbers, the multivariate linear regression model focussed only on the combined effects of time and radiation dose.

$$\Delta rCBV = a + b \times time + c \times dose + d \times time \times dose$$

A dose-correlated ΔrCBV decrease of −0.069%/Gy(RBE) was observed in the hippocampus in the multivariate analysis. In

Table 1. Patient, tumour and treatment characteristics.

Patient number [N]	
Total/male/female	14/6/8
Age at baseline [years]	
Mean ± std.	48.1 ± 13.5
Range [min – max]	[29 – 72]
Tumour characteristics [N]	
Grade: 2/3/4	3/8/3
Histology: A/AA/O/AO/GBM	1/6/2/3/3
IDH status: mutated/unmutated/unknown	7/5/2
Location: frontal/temporal/occipital	9/4/1
Hemisphere: right/left/bilateral	9/4/1
Chemotherapy [N]	
PCV/TMZ/none	6/3/5
MRI follow-up measurements	
Patients received 1/2/3 follow-ups [N]	4/6/4
Mean follow-up period [days]	221.7 ± 61.8
Range follow-up period [days]	[89 – 285]
Structures analysed at follow-up after 3/6/9 mo [N]	
Entire WM/GM	9/10/9
Amygdala	3/4/4
Caudate nucleus	1/2/2
Hippocampus	6/5/5
Pallidum	5/5/4
Putamen	1/3/4
Thalamus	3/5/4

N: number; A: astrocytoma; AA: anaplastic astrocytoma; O: oligodendroglioma; AO: anaplastic oligodendroglioma; GBM: glioblastoma; IDH: Isocitrate dehydrogenase; TMZ: temozolomid; PCV: procarbazine, lomustine and vincristine; mo: months; GM: grey matter; WM: white matter.

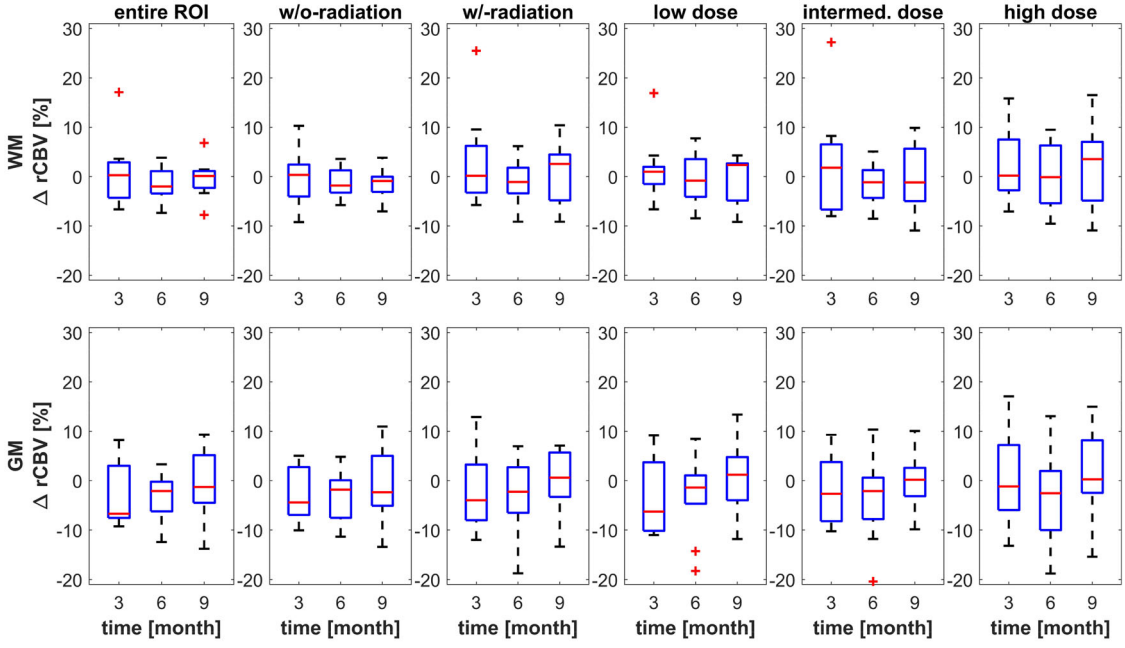

Figure 2. The percentage difference of relative cerebral blood volume (ΔrCBV) for different regions of normal-appearing white matter (WM) and grey matter (GM) is shown as boxplots for the follow-up measurement three, six and nine months after radiotherapy. The regions are divided into their prescribed dose [entire ROI: 0–60 Gy(RBE), w/o-radiation: 0–1 Gy(RBE), w/-radiation: 1–60 Gy(RBE), low dose: 1–20 Gy(RBE), intermediate dose: 21–40 Gy(RBE), high dose: 41–60 Gy(RBE)]. The boxplots show the median, lower and upper quartile, minimum, maximum and outliers. No significant alterations of the follow-up measurements with $p \leq 0.05$ were observed in any region according to the one-sided Wilcoxon signed rank test.

Table 2. Multivariate linear regression of combined data from dose-separated regions of normal-appearing white matter (WM) and grey matter (GM).

	WM			GM		
Parameter	Coefficient	Std.-error	*p*-Value	Coefficient	Std.-error	*p*-Value
Intercept [%]	$a = 1.93$	1.05	0.07	$a = 0.5$	0.8	0.51
Time [%/days]	$b = -0.006$	0.005	0.14	$b = -0.005$	0.009	0.53
Dose [%/Gy(RBE)]	$c = 0.014$	0.012	0.23	$c = 0.027$	0.009	0.001*
Gender 'f' [%]	$d = -2.66$	1.26	0.04*	$d = -2.82$	1.18	0.02*
Time × dose × gender 'f' [%/days × Gy(RBE)]	$e = -0.0001$	0.0002	0.68	$e = -0.0004$	0.0002	0.03*
Time × dose × gender 'm' [%/days × Gy(RBE)]	$f = 0.0004$	0.0002	0.008*	$f = 0.0004$	0.0003	0.27

Results from the multivariate linear regression model $\Delta rCBV = a + b \times time + c \times dose + d \times gender + e \times time \times dose \times gender\ 'f' + f \times time \times dose \times gender\ 'm'$ fitted to the combined ΔrCBV values of the low, intermediate and high dose area of normal-appearing white matter (WM) and grey matter (GM). Significant findings with a *p*-value of 0.05 are marked by *.

the thalamus, ΔrCBV correlated significantly with dose by −0.057%/Gy(RBE) and time × dose by −0.001%/days × Gy(RBE) (Table 3).

Discussion

The analyses of our data showed stable perfusion values in each GM and WM region of the NA tissue of grade 2–4 glioma patients in the follow-up period of up to nine months after proton beam irradiation. In contrast to our findings, several previous studies revealed a significant and mostly dose-dependent perfusion decrease after photon beam irradiation [16–18]. Fuss et al. [16] reported on reduced CBV in the 40–100% isodose volume of WM and GM after photon irradiation in a cohort of 25 brain tumour patients. Petr et al. [18] observed a significant CBF decrease of −16.8% in high dose (>50 Gy) and of −2.3% in low dose (<10 Gy) regions of GM in 24 glioblastoma patients three months after photon irradiation. The evaluation of absolute rather than relative parameters in both studies may explain the different outcomes compared to our study [16,18]. Fahlström et al. [17] reported significant rCBV and rCBF decreases in global GM up to three months after photon irradiation, whereas perfusion decrease in WM was significant only up to the first month after RT. Concordant with our results, no significant changes were measured in dose-separated regions. Nilsen et al. [38] assessed perfusion changes in the combined normal white and grey matter during a long observational period of up to 18 months after stereotactic radiosurgery (SRS) using gradient and spin echo to distinguish between the total vasculature and the micro-vasculature. Interestingly, significant rCBV and rCBF changes were only observed using a spin echo and not a gradient echo sequence, which corresponds to our results. However, the evaluation of the combined WM and GM area reduces the comparability of our study. By now the only study examining perfusion alterations in NA tissue after proton beam irradiation was published by Petr et al. [23] comparing the effect of proton and photon irradiation on perfusion of the NA brain tissue. While they observed a significant GM rCBF decrease in 44 patients irradiated with photons, the rCBF decrease measured in 16 proton therapy patients did not reach statistical significance. This is in accordance with our results, even if the extent of perfusion decrease measured by Petr et al. [23] was greater (–8.8 − –9.1%) than in our study. Since the rCBF decrease was independent of the radiation modality, they attributed the lack of significance after proton beam irradiation to the small number of patients, which was comparable to our cohort size. The perfusion in dose-separated regions was not evaluated for the proton patient cohort due to the small number of voxels contributing to those regions [23]. Conversely, in our analysis, we increased the number of contributing voxels by choosing broader dose steps.

The substantial difference between our and most of the above-mentioned studies is the exclusive evaluation of tissue changes after proton beam irradiation. Due to the compressed dose distribution, the normal tissue is less affected by radiation when treated with protons, which explains the stable perfusion values in the entire WM and GM dominated by the "w/o-radiation" region. The absence of perfusion alterations in the areas irradiated by a non-negligible proton dose (low, intermediate, high and "w/-radiation" area) contrasts the previous findings of dose-dependent perfusion alterations after photon irradiation. This finding leads to the conclusion that the volume of the normal-appearing brain affected by radiation dose during proton therapy may be small enough not to cause any vascular damage. The brain being a serial organ requires a certain volume to be affected by a certain radiation dose in order to cause impairment [39,40]. The time correlation in the "w/o-radiation"-region does not correspond to our expectations. However, since all measurements were performed on the same MR scanner using the identical protocol, inter-patient variability can be discarded for an explanation. The individual ageing process of each patient during the follow-up period may be a contributing factor. Unfortunately, we did not acquire perfusion scans in a cohort of healthy volunteers in order to clarify this finding.

The multivariate regression of the combined dataset of low, intermediate and high dose GM regions showed a positive correlation of ΔrCBV with dose, which is in contrast to previous publications reporting on a pronounced perfusion decrease in areas of higher radiation dose [16,18]. From the relative ΔrCBV in Figure 2 and the dose correlation shown in Suppl. Table S3 it can be concluded that the positive dose correlation was mainly due to the median ΔrCBV being lower in the low dose region than in the intermediate and high dose regions three months after RT. The occurrence of the dose-dependent correlation solely in the GM may be attributed to the different radiosensitivity of the blood vessels. The WM contains fewer larger blood vessels, whereas the GM consists of a large number of branched small capillaries, which are more radiosensitive [38,41].

Table 3. Univariate and multivariate linear regression of combined ΔrCBV data from the ipsi- and contralateral hemispheres of all subcortical GM structures.

		Amygdala			Hippocampus			Pallidum			Putamen			Thalamus		
	Parameter	Coefficient	Std.-error	*p*-Value	Coefficient	Std.-error	*p*-Value	Coefficient	Std.-error	*p*-Value	Coefficient	Std.-error	*p*-Value	Coefficient	Std.-error	*p*-Value
Univariate	Time [%/days]	$b = 0.01$	0.04	0.75	$b = -0.006$	0.014	0.67	$b = 0.001$	0.013	0.92	$b = 0.042$	0.023	0.07	$b = 0.011$	0.009	0.18
	Dose [%/Gy(RBE)]	$b = -0.38$	1.05	0.72	$b = -0.006$	0.10	0.96	$b = -0.04$	0.10	0.66	$b = 0.008$	0.028	0.78	$b = 0.04$	0.07	0.51
	Age [%/year]	$b = 0.74$	0.29	0.79	$b = -0.13$	0.08	0.11	$b = 0.08$	0.06	0.14	$b = 0.27$	0.05	$<0.001^*$	$b = -0.03$	0.06	0.57
	Gender 'f'	$b = -20.20$	3.29	$<0.001^*$	$b = -11.6$	1.9	$<0.001^*$	$b = -0.2$	1.6	0.89	$b = 1.7$	2.5	0.49	$b = -2.9$	1.4	0.04^*
	Tumour grade 'LG'	$b = -8.62$	4.26	0.04^*	$b = 3.71$	2.21	0.10	$b = 0.2$	0.9	0.85	$b = 3.7$	2.5	0.13	$b = -$	–	–
	Chemotherapy 'yes'	$b = -1,1$	7.0	0.88	$b = 2.4$	2.9	0.40	$b = -1.11$	1.21	0.36	$b = -4.4$	3.7	0.22	$b = -1.4$	1.7	0.41
Multivariate	Intercept [%]	$a = -0.8$	2.8	0.76	$a = 0.3$	1.0	0.72	$a = -2.33$	2.04	0.25	$a = -5.6$	1.015	0.82	$a = 1.82$	1.11	0.10
	Time [%/days]	$b = 0.01$	0.05	0.84	$b = 0.002$	0.013	0.90	$b = 0.006$	0.015	0.69	$b = -0.05$	0.026	0.22	$b = 0.0003$	0.011	0.98
	Dose [%/Gy(RBE)]	$c = -0.7$	0.9	0.43	$c = -0.069$	0.029	0.02^*	$c = -0.001$	0.08	0.98	$c = 0.12$	0.023	0.14	$c = -0.057$	0.022	0.01^*
	Time × dose [%/days × Gy(RBE)]	$d = 0.002$	0.014	0.90	$d = -0.001$	0.0008	0.42	$d = -0.0004$	0.0008	0.61	$d = -0.002$	0.0004	0.13	$d = -0.001$	0.0003	0.04^*

Results from the univariate and multivariate linear regression models fitted to the combined ΔrCBV values of ipsi- and contralateral hemisphere of all subcortical GM structures. Univariate model: $\Delta rCBV = a + b \times parameter$, multivariate model: $\Delta rCBV = a + b \times time + c \times dose + d \times time \times dose$. Significance is reached at a *p*-value of 0.05 marked by *.

An additional factor to be considered when comparing our results to previous studies is the potential impact of atrophy. Several studies confirmed the appearance of brain atrophy in WM, GM and specific subcortical GM structures after radiotherapy [23,36,42–44]. Petr et al. [23] reported significant WM and GM atrophy only after photon, but not proton therapy. Radiation-induced atrophy may have influenced findings in previous studies and thus could explain the different results. Noteworthy, we applied a 95% probability threshold for the WM and GM masks to reduce the possible impact of atrophy on our results.

The limitations of our study include the small number of patients, especially when evaluating the perfusion changes in the subcortical GM structures. Due to the limited patient number and the sensitivity to outliers in the relatively small subcortical GM regions, the results indicating no radiation-induced damage in these regions should be considered with caution. Another limitation may be the multimodal transformation between CT and MRI and the registration of MRI contrasts, leading to the misidentification of tissue structures. To prevent registration uncertainties, we considered several registration options and found the transformation from T1w map to the rCBV map to be the most suitable. The impact of outliers could further be reduced by improving the registration with the help of a B0- and susceptibility correction in future studies. Moreover, the impact of LET on the evaluation of radiation-induced changes is of interest to our group [45,46] but was not conducted due to the small cohort size and the scope of this manuscript. Finally, the heterogeneity of tumour characteristics, i.e. grade and mutation, may cause a different response on MR imaging. Due to the small cohort size, a detailed analysis of the individual characteristics was not possible.

In summary, our data showed no significant perfusion changes in the observational period up to nine months after proton beam irradiation. To study the different radiosensitivity of normal tissue changes after proton and photon beam irradiation and its effect on neuro-cognition, a larger patient cohort treated with any of the two radiation modalities and evaluated with a cognitive function test is warranted.

Acknowledgments

We thank all patients and healthy volunteers for participating in the respective studies. Moreover, Philips (Eindhoven, The Netherlands) is acknowledged for providing Research Keys for the 3T Ingenuity PET/MR scanner, with which the advanced images were obtained. Finally, this work was partly funded by the National Center for Tumor Diseases (NCT), Partner Site Dresden.

Disclosure statement

The authors have no financial or proprietary interests in any material discussed in this article.

Funding

No funding was received to assist with the preparation of this manuscript.

ORCID

Katharina Witzmann http://orcid.org/0000-0002-1939-6530

Data availability statement

Raw data were generated at the University Hospital Carl Gustav Carus, Department of Radiotherapy and Radiation Oncology and stored in the institutional database RadPlanBio. Derived data supporting the findings of this study are available from the corresponding author E.G.C. Troost on request.

References

[1] Wesseling P, Capper D. WHO 2016 classification of gliomas. Neuropathol Appl Neurobiol. 2018;44(2):139–150.
[2] Louis DN, Perry A, Reifenberger G, et al. The 2016 world health organization classification of tumors of the central nervous system: a summary. Acta Neuropathol. 2016;131(6):803–820.
[3] Weller M, van den Bent M, Preusser M, et al. EANO guidelines on the diagnosis and treatment of diffuse gliomas of adulthood. Nat Rev Clin Oncol. 2021;18(3):170–186.
[4] van den Bent MJ, Afra D, de Witte O, et al. Long-term efficacy of early versus delayed radiotherapy for low-grade astrocytoma and oligodendroglioma in adults: the EORTC 22845 randomised trial. Lancet. 2005;366(9490):985–990.
[5] Niyazi M, Brada M, Chalmers AJ, et al. ESTRO-ACROP guideline target delineation of glioblastomas. Radiother Oncol. 2016;118(1):35–42.
[6] Dirven L, Reijneveld JC, Taphoorn MJB, et al. Impact of radiation target volume on health-related quality of life in patients with low-grade glioma in the 2-year period post treatment: a secondary analysis of the EORTC 22033–26033. Int J Radiat Oncol Biol Phys. 2019;104(1):90–100.
[7] Greene-Schloesser D, Robbins ME, Peiffer AM, et al. Radiation-induced brain injury: a review. Front Oncol. 2012;2:73.
[8] Makale MT, McDonald CR, Hattangadi-Gluth JA, et al. Mechanisms of radiotherapy-associated cognitive disability in patients with brain tumours. Nat Rev Neurol. 2017;13(1):52–64.
[9] Sheline GE, Wara WM, Smith V. Therapeutic irradiation and brain injury. Int J Radiat Oncol Biol Phys. 1980;6(9):1215–1228.
[10] Prasanna PG, Rawojc K, Guha C, et al. Normal tissue injury induced by photon and proton therapies: gaps and opportunities. Int J Radiat Oncol Biol Phys. 2021;110(5):1325–1340.
[11] Tringale KR, Nguyen TT, Karunamuni R, et al. Quantitative imaging biomarkers of damage to critical memory regions are associated with post-radiation therapy memory performance in brain tumor patients. Int J Radiat Oncol Biol Phys. 2019;105(4):773–783.
[12] Yang J, Xu Z, Gao J, et al. Evaluation of early acute radiation-induced brain injury: hybrid multifunctional MRI-based study. Magn Reson Imaging. 2018;54:101–108.
[13] Raschke F, Wesemann T, Wahl H, et al. Reduced diffusion in normal appearing white matter of glioma patients following radio(-chemo)therapy. Radiother Oncol. 2019;140:110–115.
[14] Kłos J, van Laar PJ, Sinnige PF, et al. Quantifying effects of radiotherapy-induced microvascular injury; review of established and emerging brain MRI techniques. Radiother Oncol. 2019;140:41–53.
[15] Estève F, Rubin C, Grand S, et al. Transient metabolic changes observed with proton MR spectroscopy in normal human brain after radiation therapy. Int J Radiat Oncol Biol Phys. 1998;40(2):279–286.
[16] Fuss M, Wenz F, Scholdei R, et al. Radiation-induced regional cerebral blood volume (rCBV) changes in normal brain and low-grade astrocytomas: quantification and time and dose-dependent occurrence. Int J Radiat Oncol Biol Phys. 2000;48(1):53–58.
[17] Fahlström M, Blomquist E, Nyholm T, et al. Perfusion magnetic resonance imaging changes in normal appearing brain tissue after radiotherapy in glioblastoma patients may confound longitudinal evaluation of treatment response. Radiol Oncol. 2018;52:143–151.
[18] Petr J, Platzek I, Seidlitz A, et al. Early and late effects of radiochemotherapy on cerebral blood flow in glioblastoma patients measured with non-invasive perfusion MRI. Radiother Oncol. 2016;118(1):24–28.
[19] Price SJ, Jena R, Green HA, et al. Early radiotherapy dose response and lack of hypersensitivity effect in normal brain tissue: a sequential dynamic susceptibility imaging study of cerebral perfusion. Clin Oncol (R Coll Radiol). 2007;19(8):577–587.
[20] Jakubovic R, Sahgal A, Ruschin M, et al. Non tumor perfusion changes following stereotactic radiosurgery to brain metastases. Technol Cancer Res Treat. 2015;14(4):497–503.
[21] Lee MC, Cha S, Chang SM, et al. Dynamic susceptibility contrast perfusion imaging of radiation effects in normal-appearing brain tissue: changes in the first-pass and recirculation phases. J Magn Reson Imaging. 2005;21(6):683–693.
[22] Fahlström M, Fransson S, Blomquist E, et al. Dynamic contrast-enhanced magnetic resonance imaging may act as a biomarker for vascular damage in normal appearing brain tissue after radiotherapy in patients with glioblastoma. Acta Radiol Open. 2018;7(11):2058460118808811.
[23] Petr J, Platzek I, Hofheinz F, et al. Photon vs. proton radiochemotherapy: Effects on brain tissue volume and perfusion. Radiother Oncol. 2018;128(1):121–127.
[24] Avants BB, Tustison NJ, Stauffer M, et al. The insight ToolKit image registration framework. Front Neuroinform. 2014;8:44.
[25] Fonov V, Evans AC, Botteron K, et al. Unbiased average age-appropriate atlases for pediatric studies. Neuroimage. 2011;54(1):313–327.
[26] Jenkinson M, Beckmann CF, Behrens TE, et al. FSL. Neuroimage. 2012;62(2):782–790.
[27] Ashburner J, Barnes G, Chen C-C et al. SPM12 Manual. London: UCL Queen Square Institute of Neurology; 2021. Available from: https://www.fil.ion.ucl.ac.uk/spm/
[28] Fisel CR, Ackerman JL, Buxton RB, et al. MR contrast due to microscopically heterogeneous magnetic susceptibility: numerical simulations and applications to cerebral physiology. Magn Reson Med. 1991;17(2):336–347.
[29] Rosen BR, Belliveau JW, Chien D. Perfusion imaging by nuclear magnetic resonance. Magn Reson Q. 1989;5(4):263–281.
[30] Thompson HK, Starmer CF, Whalen RE, et al. Indicator transit time considered as a gamma variate. Circ Res. 1964;14:502–515.
[31] Yin J, Yang J, Guo Q. Automatic determination of the arterial input function in dynamic susceptibility contrast MRI: comparison of different reproducible clustering algorithms. Neuroradiology. 2015;57:535–543.
[32] Mouridsen K, Christensen S, Gyldensted L, et al. Automatic selection of arterial input function using cluster analysis. Magn Reson Med. 2006;55(3):524–531.
[33] MATLAB. 9.7.0.1190202 (R2019b). Natick, Massachusetts: the MathWorks Inc.; 2018.
[34] Axel L. Cerebral blood flow determination by rapid-sequence computed tomography: theoretical analysis. Radiology. 1980;137(3):679–686.
[35] Raschke F, Witzmann K, Seidlitz A, et al. Time- and dose-dependent volume decreases in subcortical grey matter structures of glioma patients after radio(chemo)therapy. Clin Transl Radiat Oncol. 2022;36:99–105.
[36] Nagtegaal SHJ, David S, Philippens MEP, et al. Dose-dependent volume loss in subcortical deep grey matter structures after cranial radiotherapy. Clin Transl Radiat Oncol. 2021;26:35–41.
[37] IBM SPSS statistics for windows. Armonk, NY: IBM Corp.; Released 2021.
[38] Nilsen LB, Digernes I, Grøvik E, et al. Responses in the diffusivity and vascular function of the irradiated normal brain are seen up

until 18 months following SRS of brain metastases. Neurooncol Adv. 2020;2(1):vdaa028.
[39] Kirkpatrick JP, Marks LB, Mayo CS, et al. Estimating normal tissue toxicity in radiosurgery of the CNS: application and limitations of QUANTEC. J Radiosurg SBRT. 2011;1(2):95–107.
[40] Lawrence YR, Li XA, el Naqa I, et al. Radiation dose-volume effects in the brain. Int J Radiat Oncol Biol Phys. 2010;76(3 Suppl):S20–S27.
[41] Dimitrievich GS, Fischer-Dzoga K, Griem ML. Radiosensitivity of vascular tissue. I. Differential radiosensitivity of capillaries: a quantitative *in vivo* study. Radiat Res. 1984;99(3):511–535.
[42] Raschke F, Seidlitz A, Wesemann T, et al. Dose dependent cerebellar atrophy in glioma patients after radio(chemo)therapy. Radiother Oncol. 2020;150:262–267.
[43] Takeshita Y, Watanabe K, Kakeda S, et al. Early volume reduction of the hippocampus after whole-brain radiation therapy: an automated brain structure segmentation study. Jpn J Radiol. 2020; 38(2):118–125.
[44] Gommlich A, Raschke F, Wahl H, et al. Retrospective assessment of MRI-based volumetric changes of normal tissues in glioma patients following radio(chemo)therapy. Clin Transl Radiat Oncol. 2018;8:17–21.
[45] Peeler CR, Mirkovic D, Titt U, et al. Clinical evidence of variable proton biological effectiveness in pediatric patients treated for ependymoma. Radiother Oncol. 2016;121(3):395–401.
[46] Eulitz J, Troost EGC, Klünder L, et al. Increased relative biological effectiveness and periventricular radiosensitivity in proton therapy of glioma patients. Radiother Oncol. 2022;178:109422.